Energy Storage Materials 51 (2022) 97–107

Contents lists available at ScienceDirect

Energy Storage Materials

journal homepage: www.elsevier.com/locate/ensm

Lithium-sulfur battery diagnostics through distribution of relaxation times analysis

Roby Soni [a,b], James B. Robinson [a,b], Paul R. Shearing [a,b], Dan J.L. Brett [a,b], Alexander J.E. Rettie [a,b,*], Thomas S. Miller [a,b,*]

[a] Department of Chemical Engineering, Electrochemical Innovation Lab, University College London, London WC1E 7JE, UK
[b] The Faraday Institution, Quad One, Harwell Science and Innovation Campus, Didcot OX11 0RA, UK

A B S T R A C T

Electrochemical impedance spectroscopy (EIS) is widely used in battery analysis as it is simple to implement and non-destructive. However, the data provided is a global representation of all electrochemical processes within the cell and much useful information is ambiguous or inaccessible when using traditional analysis techniques. This is a major challenge when EIS is used to analyse systems with complex cell chemistries, like lithium-sulfur (Li-S), one of the strongest candidates to supersede conventional Li-ion batteries. Here we demonstrate the application of distribution of relaxation times (DRT) analysis for quantitative deconvolution of EIS spectra from Li-S batteries, revealing the contributions of (eight) distinct electrode processes to the total cell polarisation. The DRT profile is shown to be strongly dependent on cell state-of-charge, offering a route to automated and on-board analysis of Li-S cells.

1. Introduction

Lithium-sulfur (Li-S) batteries have emerged as one of the most promising 'beyond Li-ion' technologies due to the high theoretical capacity [1] (1675 mAh g^{-1}), low cost and low toxicity of sulfur as a positive electrode material. Although capacities close to the theoretical values in the initial cycles have been attained [2–4], rapid capacity fade and poor rate capability are significant bottlenecks that prevent widespread commercialisation [5–7].

A Li-S battery, typically consisting of a lithium negative electrode and carbon-supported sulfur composite positive electrode, undergoes numerous complex cell reactions during operation. On discharge, elemental sulfur is converted to Li_2S, proceeding via the formation of a series of different intermediate polysulfides (PSs), including Li_2S_8, Li_2S_6, Li_2S_4, Li_2S_2 [8], with the reverse theoretically occurring during charge. However, many of these PSs are soluble, meaning species formed at the S positive electrode are transported to the Li negative electrode during cycling, where they can be reduced to Li_2S or soluble shorter-chain PSs that can travel back to the S electrode to be further reduced (on discharge) or re-oxidised (on charge). This PS 'shuttling' results in the loss of active sulfur and capacity fade during cycling. The complexity of this chemistry makes the non-destructive diagnosis of cell processes and performance a highly challenging task. Careful analysis of these cell processes during operation is imperative for addressing performance-limiting steps.

In situ analysis of batteries at different states-of-charge (SoC) can provide a wealth of information about the processes that drive degradation and failure and hence, help promote cell stability and prolong cycle life. Among the *in situ* techniques available, electrochemical impedance spectroscopy (EIS) is powerful due to its non-destructive nature and ability to provide information about electrode processes in real-time under normal operating conditions [9a,b].

EIS has been widely utilised to study Li-S batteries and factors such as cell SoC [10], temperature [11] and state-of-health [12], have been shown to impact the spectra obtained. Early studies were performed by Cãnas et al. [10], who proposed an equivalent circuit model (ECM) quantifying different electrochemical processes in their cells at different SoC. They assigned the high-frequency semicircle of their Nyquist plots (real vs. imaginary components of the complex impedance) to charge transfer reactions at the negative electrode, while mid-frequency loops were attributed to positive electrode reactions, mainly the charge transfer reaction of sulfur intermediates and the formation and dissolution of S_8 and Li_2S. However, other studies performed at a similar time drew different conclusions. For example, Deng et al. [11], who also measured EIS at different SoC as well as measuring the temperature dependence, attributed the mid-frequency semi-circle to charge transfer processes and their relative capacitance and the high-frequency semi--circle to the interfacial contact resistance in the sulfur electrode bulk. Cãnas et al. [10] assigned these same features to the formation and dissolution of S_8 and Li_2S or charge transfer of sulfur intermediates, and

* Corresponding authors at: Department of Chemical Engineering, Electrochemical Innovation Lab, University College London, London WC1E 7JE, UK.
E-mail addresses: a.rettie@ucl.ac.uk (A.J.E. Rettie), t.miller@ucl.ac.uk (T.S. Miller).

https://doi.org/10.1016/j.ensm.2022.06.016
Received 28 March 2022; Received in revised form 11 May 2022; Accepted 11 June 2022
Available online 17 June 2022

anodic interfacial charge transfer, respectively. Similarly, Yan et al. [13]. studied Li-S cell capacity fade using EIS, comparing the effect of the electrolyte:sulfur ratio. Once again, the conclusions drawn regarding the contributions to the Nyquist plots were different, with the semicircle in the high-frequency region attributed to charge-transfer processes at the carbon (positive electrode) interface, while the semicircle in the medium-frequency region was related to the formation of solid Li_2S_2/Li_2S films. More recently, Kilic and Eroglu [14] studied the effect of cell design on the EIS of Li-S batteries, in their analysis they observed two semi-circles and a diffusion feature in their Nyquist plot, which they assigned purely to positive electrode reactions. Nonetheless, despite the inconsistency in interpretation, these studies do highlight the fact that EIS has great potential to non-destructively diagnose processes within operational Li-S cells.

An EIS spectrum is a global representation of the relaxation processes occurring in the system under consideration. Unfortunately, conventional EIS analysis, i.e., equivalent circuit modelling, is often unable to resolve or distinguish between the relaxation processes taking place in overlapping frequency ranges [15]. Battery studies using EIS have commonly used complex non-linear square (CNLS) circuit fitting, which is mostly intuitive and based on the features of impedance data, introducing a high likelihood of missing overlapping processes or those that occur at close time constants. Analysis is even more challenging for complex systems like Li-S batteries, where multiple reactions occur at the positive and negative electrodes leading to the formation of different products. An alternative approach is to transform the EIS data, which is a function of frequency, into the time domain, also known as the distribution of relaxation times (DRT). In DRT analysis, the EIS spectrum is fitted with an infinite Voight circuit (a series of parallel *RQ* elements, where *R* is a resistor and *Q* is a constant phase element) where each *RQ* element represents a time constant $\{\tau = (RQ)^{1/\alpha}\}$, where τ is the time constant, and α is a number between 0 and 1 [16,17]. Hence, DRT analysis can resolve overlapping relaxation processes into a series of local maxima where each maximum represents an electrochemical process. This allows subtle changes in the EIS data to be resolved. The peak area, position and height can provide quantitative information about the reaction kinetics and performance-limiting processes [18]. DRT was first applied by Franklin and De Bruin to analyse impedance data of solid-state electrolytes [19] and it has become increasingly popular for device studies in the last 20 years, being successfully applied to solid oxide fuel cells [20–22], polymer electrolyte membrane fuel cells [23–25], and Li-ion batteries [26,27], revealing internal phenomena during operation. A small number of studies have previously utilised DRT to deconvolute select EIS data from LiS batteries to deliver insights into factors including cell capacity fade processes [28a] the effect of electrode microstructure on performance [28b], or the dynamics of interfacial processes [28c]. Unfortunately these studies commonly rely soley on symmetric C||C or CS||CS systems [28b], or primary focus on the contribution of PSs [28c], only one of many important comstituents in Li-S batteries. Where full cells have been tested, the assignment of DRT features has largely been achieved through the use of literature data or predicted time constants, rather than through empirical experiments using equivalent cells or electrodes, and many known Li-S cell processes could not be linked to the DRT signature [28a,29].

In this work, we apply DRT analysis to full Li-S batteries based on commercial positive electrodes, allowing in-depth analysis and diagnosis of cell SoC, as well as identifying performance-limiting processes. DRT features are shown to have a strong and characteristic dependence on cell properties and importantly eight unique polarisation resistances that comprise the EIS spectrum are identified and experimentally assigned to distinct cell reactions, with significant implications of Li-S battery diagnostics. The effects of different electrolyte conditions are also demonstrated.

2. Material and methods

2.1. Materials

Nanomyte BE-70 sulfur positive electrodes were purchased from the NEI Corporation. The electrodes, composed of 70 wt.% sulfur, 10 wt.% polyvinylidene fluoride binder and 20 wt.% carbon black, were used as received. The active loading of sulfur was 3.7 mg cm^{-2} (thickness 55 μm). Lithium disks (15.6 mm diameter and 0.45 mm thickness) were procured from PI-KEM Ltd. For electrolyte preparation, 1, 3-dioxolane (DOL), 1, 2-dimethoxyethane (DME) solvents, lithium bis(trifluoromethanesulfonyl)imide (LiTFSI), and lithium nitrate ($LiNO_3$) salts were supplied by Sigma-Aldrich.

2.2. Cell fabrication

For cell fabrication, pre-dried sulfur electrodes were cut into 14 mm diameter disks inside an argon-filled glovebox (MBraun, O_2 and H_2O levels < 0.5 ppm). Two-electrode CR2032 coin cells were constructed by stacking a Li disk (2072% excess), separator (Celgard-2400, 25 μm) and a sulfur positive electrode, before an electrolyte containing 1 M LiTFSI and 1 M $LiNO_3$ in a 1:1 v/v mixture of DOL/DME was added. Two 0.5 mm spacers and a spring (1.2 mm high and 0.3 mm thick) were used in the cell. Cells with an electrolyte to sulfur (ES) ratio of 5 μL/mg_{Sulfur} (lean electrolyte, ES-5) and 15 μL/mg_{Sulfur} (flooded electrolyte, ES-15) were used to analyse the effect of electrolyte volume on the cell performance. Symmetric Li||Li and S||S cells were also assembled using the same process, but in these cases, 50 μL of electrolyte was used. For recording the impedance of PS solutions, symmetric cells were fabricated with carbon paper (AvCarb P50) electrodes and 10 mM Li_2S_6 and Li_2S_4 dissolved in the aforementioned electrolyte. For the preparation of PS-electrolyte solutions, a 1 M solution of Li_2S_6 and Li_2S_4, respectively, were prepared by dissolving an appropriate amount of Li_2S and S in DOL at 50 °C in an argon-filled glove box. From these solutions the required amount of PS was added into the electrolyte. A PS infused electrolyte (10 mM Li_2S_6) was used in the symmetric Li||Li cell to analyse the effect of PSs at the electrode.

2.3. Electrochemical tests and DRT analysis

All the electrochemical measurements were carried out using a VSP Biologic multichannel potentiostat at room temperature. EIS measurements were performed under open-circuit conditions with an applied amplitude of 5 mV, measurements were made in the frequency range of 50 mHz to 1 MHz (swept from high to low frequency) and 10 points per decade were recorded during each measurement. Cells were rested for 2 h post-fabrication to allow electrode wetting. Formation cycles were performed by first discharging the cell to 1.8 V at C/20 (C = 1675 mAh g^{-1}), before a full charge-discharge cycle at C/20 in the voltage range of 1.8–2.6 V was performed. After formation, EIS measurements were performed during discharge at different SoC (from 100% to 0%). The cells were brought to required SoC at a rate of C/20. The cells were kept at OCV for 30 min after bringing the cell to the desired SoC to allow the cell to achieve steady-state before EIS measurements were made.

The validity of the EIS measurements was checked by performing Kramer-Kronig analyses using ec-idea software [30]; for valid EIS data the residuals of the real and imaginary components of the impedance should be within the limit of 1% (see Supporting Information). Open-source MATLAB script-based software (DRT Tools) was used to calculate DRT from the impedance data [31]. The Tikhonov regularization was used to fit discrete experimental data in a non-linear least-square manner and the Gaussian method was used for data discretization. The experimental data were fitted using both real and imaginary components of the EIS, while the inductive data was discarded. Second-order regularization derivative fitting parameters were used and the regularization parameter was set at 0.0001 (residuals

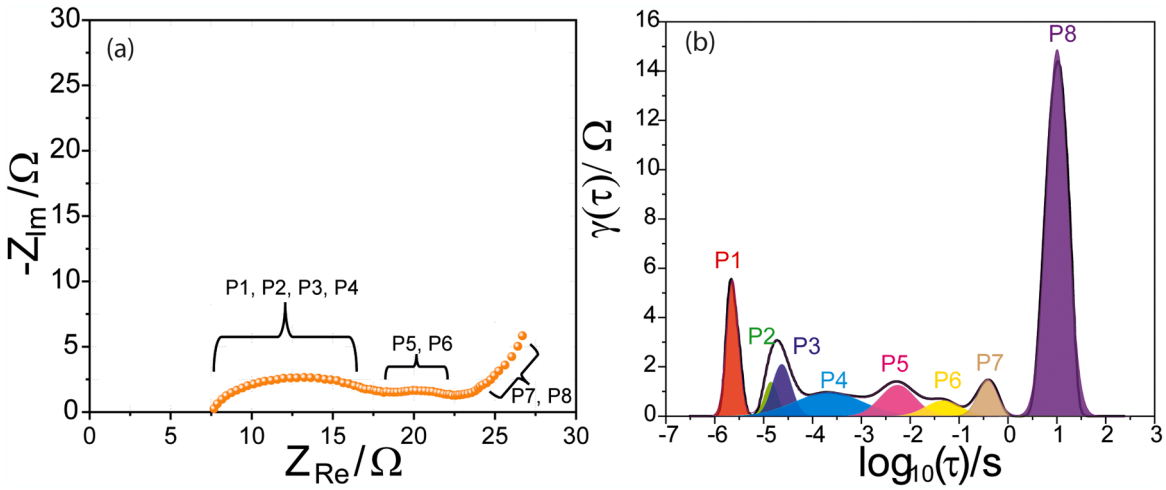

Fig. 1. (a) Nyquist plot of LiS-5 recorded at OCV at 100% SoC and (b) DRT plot of the impedance data shown in (a). The 'P' prefix is used here as the cell has undergone a formation cycle before the measurement was made.

between real impedance and impedance derived from DRT are within the acceptably low for this value), while radial basis function (RBF) with FWHM of 0.5 was used; these parameters gave appropriate fitting of the EIS data. Measured DRT were fitted with a Gaussian non-linear curve fit using the Levenberg-Marquardt iteration method in Origin to calculate the polarisation resistance and time constants. For peak fitting, the number of peaks was manually selected and the base of the peak was fixed to zero whereas other peak parameters such as position, area, and FWHM were not fixed and the iterations were performed until the convergence of fit (to reach R^2 ~1).

3. Results and discussion

3.1. Identifying relaxation processes using DRT analysis

EIS data, in the form of a Nyquist plot, for a lean electrolyte (E/S ratio = 5) Li-S cell in a fully charged state (100% SoC) recorded after a formation cycle are shown in Fig. 1a. Two semi-circles, one in the high-frequency region and one in the mid-frequency region, can be seen followed by a diffusion line in the low-frequency region. Similar features have been observed for Li-S batteries in earlier studies [11,13,32]. However, as discussed above, the assignment of these two semi-circles to specific cell processes is disputed, with many literature reports assigning the high-frequency semi-circle to negative electrode reactions and the mid-frequency semi-circle to the positive electrode reactions [32,33], whereas other studies have assigned both semi-circles to positive electrode reactions [13,34].

Fig. 1b shows the DRT plot derived from the data in Fig. 1a, featuring eight local maxima, each representing a resistance contribution of a cell process to the total polarisation resistance of the cell. The time constant (τ) is characteristic for each polarisation process and the area under the peaks represents the polarisation resistance (R_P) contribution of a specific reaction to the total cell polarisation. Therefore, changes in the DRT profile can give a direct indication of changes in the nature and magnitude of the electrode reactions. The eight peaks (P1-P8) each have a characteristic time constant; peaks P1, P2, P3 and P4 at 2.28, 14.14, 23.6 and 217 μs, respectively, represent polarisations that constitute the high-frequency semi-circle; whereas peaks P5 and P6 at time constants 5.51 and 47.5 ms represent the reactions identified in the mid-frequency semi-circle; finally, P7 and P8 at 0.384 and 10.12 s, in the low-frequency region, constitute the diffusion processes [35]. It is interesting to observe two peaks in the diffusion region as this indicates two distinct ion diffusion regimes, a phenomenon previously unidentified in Li-S batteries. Although multiple peaks were observed by Danzer in commercial Li-ion batteries pertaining to diffusion, they were assigned to a single process (solid-state diffusion) [36], in this analysis of Li-S cells it is found that the two peaks in the diffusion region represent different processes, as elaborated below. The labelling convention of P1-P8 will be used throughout where appropriate.

To elucidate the origins of P1–8, their behavior at different SoCs was monitored. A voltage-time profile of a pristine LiS-5 cell as it was discharged is given in Fig. S1a; the cell was discharged to a specific voltage representing different known cell reactions [8] and rested to reach steady-state before EIS measurements were made (Fig. S1b–g), this procedure was repeated until the cell was fully discharged. DRT analysis of this data is shown in Fig. 2. Similarly, to identify peaks belonging to negative or positive impedance contributions, complementary measurements were made on symmetric S||S cells and Li||Li (EIS Fig. S2a, b; DRT Fig. 3a, b), C paper||C paper cells with PSs (Li_2S_4 and Li_2S_6) dissolved in electrolyte (EIS Fig. S2e, f; DRT Fig. 3c, d), and Cu||Li_2S cells (Fig. S3).

In a freshly prepared cell that has not been through any formation process (at 100% SoC) only sulfur is present in the positive electrode, the electrolyte is expected to be close to the as-prepared formula and no solid electrolyte interphase|positive electrode/electrolyte interface has been formed; hence the relatively simple appearance of the DRT profile (Fig. 2a), previously reported to be characteristic of the blocking behaviour of the sulfur electrode [37]. It should be noted that the 'F' prefix is used in Fig. 2 as the time constants for the peaks are in flux and have not stabilised at their 'P' positions. This is because the electrode/electrolyte interface and electrode structure, along with the cell capacitance and resistances, evolve significantly in cells during their first (i.e., formation) cycle.

Once discharge begins the DRT becomes highly complex, as at 2.3 V sulfur is reduced to high-order PSs, e.g., Li_2S_8 and Li_2S_6 [8], which can be involved with a range of cell processes. At this SoC, modification of the positive electrode structure also takes place, giving rise to a new pore structure and the loss of electrode blocking behaviour [37]. The impact of this can be observed in the polarisation resistance linked to ion diffusion processes (F8 at 7.05 s), which significantly decreases from 162 Ω at 100% SoC to 3.70 Ω at 2.30 V (Fig. 2b). On further discharge to 2.13 V (Fig. 2c) an increase in overall polarisation resistance is observed, which may be linked to the known increase in the electrolyte viscosity at this potential as more PSs are formed and dissolve in the electrolyte [8, 13].

By 2.03 V processes including PS precipitation within the positive electrode and the formation of a Li_2S_2 layer have been observed [8], although any change in DRT here is more subtle (Fig. 2d). However by

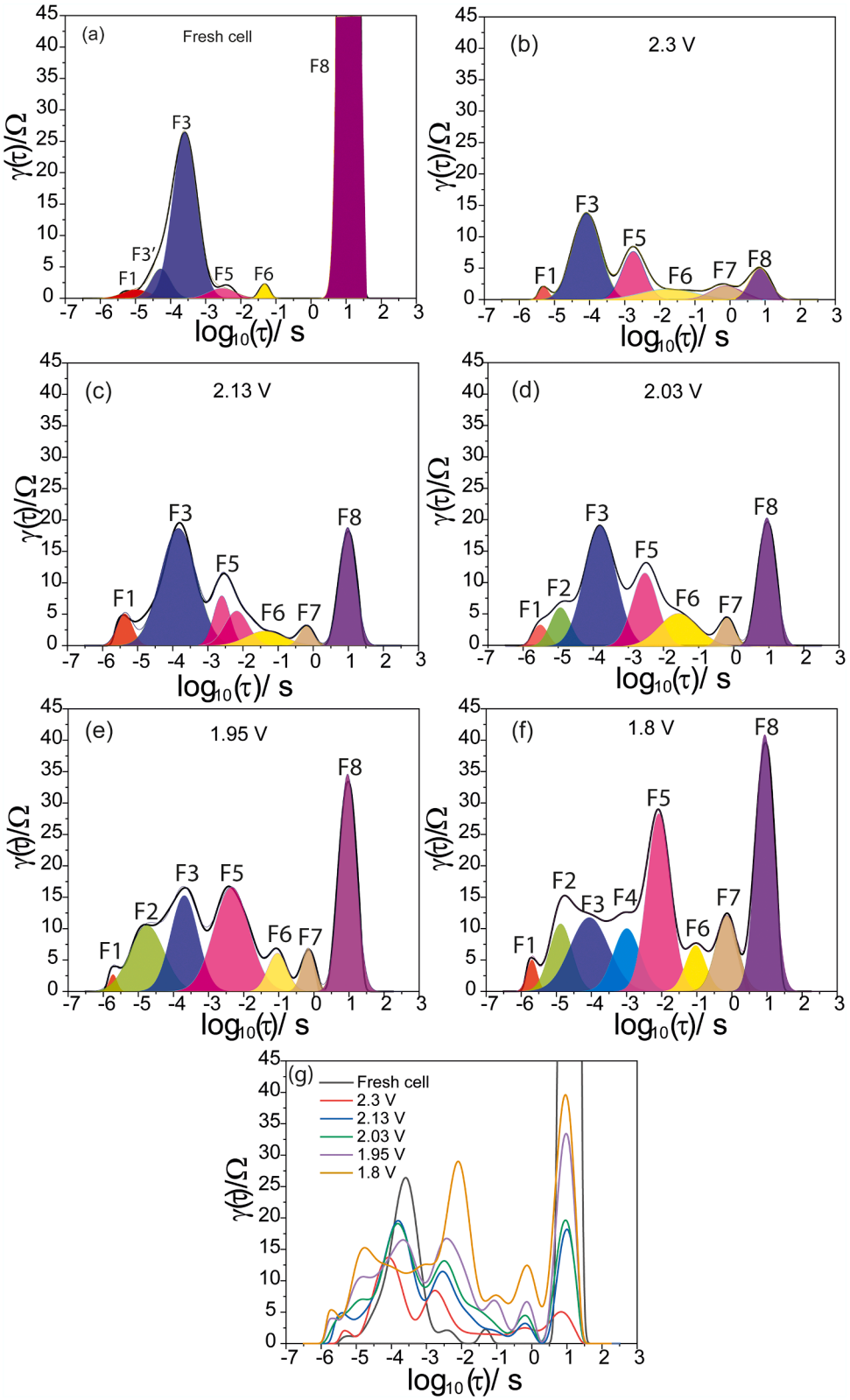

Fig. 2. DRT profiles for (a) a fresh cell at 100% SoC, then (b) discharged to 2.3 V; (c) discharged to 2.13 V; (d) discharged to 2.03 V; (e) discharged to 1.95 V and (f) fully discharged to 1.8 V. (g) Combined DRT profiles during discharge. The 'F' prefix is used here as the cell is fresh and has not undergone a formation cycle before the measurement was made.

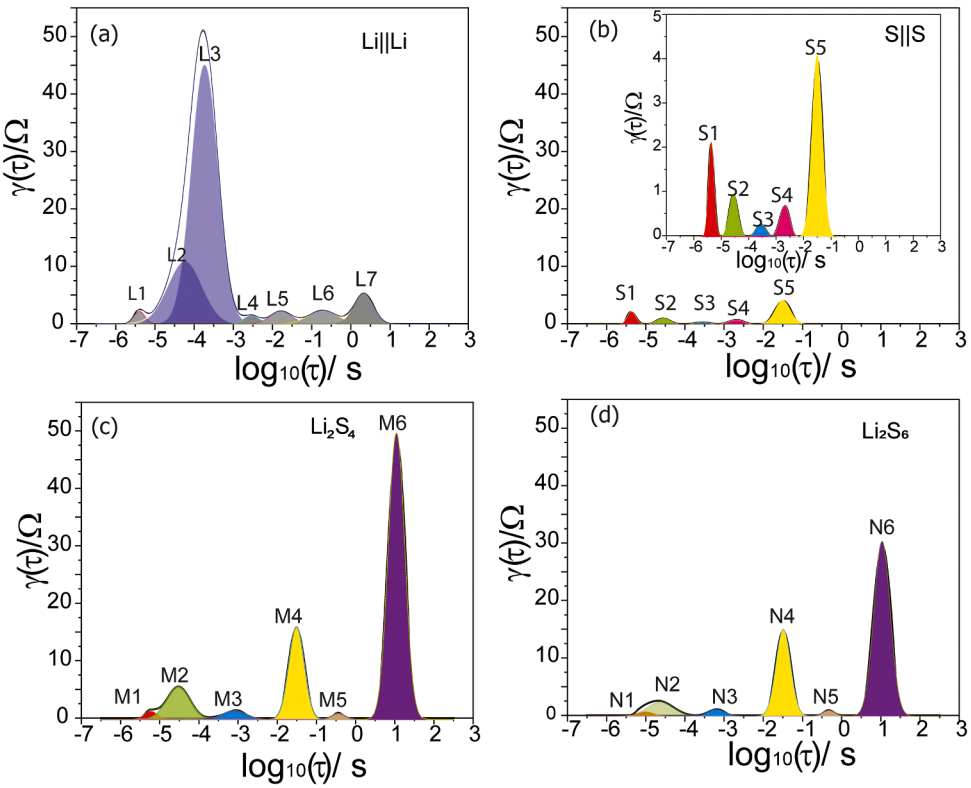

Fig. 3. DRT profiles for (a) a symmetric Li cell; (b) a symmetric sulfur cell; (c) and (d) symmetric carbon paper cells containing 10 mM Li_2S_4 and Li_2S_6 dissolved in the electrolyte.

1.95 V, a region where electronically insulating (≈10^{-9} S cm^{-1}) [38] and low ionic conductivity (10^{-13} S cm^{-1}) [39] Li_2S is formed from Li_2S_2, significant changes occur (Fig. 2e). In particular an increase in peaks F5 and F8 and a reduction in magnitude of F3. On complete discharge (1.8 V, Fig. 2f) the majority of PSs are reduced to Li_2S and here F5 and F8 increase in magnitude, along with a growth in the second diffusional peak P7.

Despite the data complexity, the DRT profiles shown in Figs. 2 and 3 can allow us to tentatively assign each of peaks P1 to P8 (Fig. 1b) to a specific cell processes, based on correlations in time constants between peaks, knowledge of dominant processes at certain potentials based on prior studies [8] and control experiments. This assignment is justified below.

The polarisation resistance of P1 shows both fast relaxation times and synchronously changes with cell equivalent series resistance (ESR), which represents the total Ohmic resistance with contributions from ionic resistance and electronic resistance of the electrodes, upon discharge. It can hence be preliminarily assigned to inter-particle/ distributed Ohmic resistances resulting from the interplay of ionic resistance in the electrolyte and electronic resistance in the porous electrode [18], which exhibits a frequency dispersion due non-uniformity of particle sizes and their distribution in the porous electrode.

No peak with a time constant close to that of P2 can be resolved in the freshly prepared cell (Fig. 2a); contributions in this region only become significant once the cell drops below 2.03 V (Fig. 2d), where processes including PS precipitation within the positive electrode and the formation of a Li_2S_2 layer are known to occur [8]. Significant contributions are however retained at lower potentials (Fig. 2d, e) and also occur in the cell at 100% SoC after formation (Fig. 1b). A similar peak appears at the same time constant (29.97 μs) in the DRT of the S||S symmetric cell (Fig. 3b), the C||C cell with PS-infused electrolyte (Fig. 3c, d) and a Li-S cell at 0% SoC (Fig. S4), but not the Li||Li cell. This observation suggests these peaks primarily derive from a positive electrode contribution. As the region of the EIS spectrum where **P2** appears is one where double layer relaxations are known to be dominant [36], it is also highly likely this type of contribution leads to this peak. Hence we attribute it to double-layer relaxations at the positive electrode.

The origin of **P3** is indicated in the features observed in the fresh cell (Fig. 2a) and the symmetric Li||Li cell (Fig. 3a). The DRT profiles of both cells are strikingly similar, displaying a large peak close to 250 μs, demonstrating that the EIS response of the fresh Li||S cell is dominated by the Li negative electrode; the Nyquist plot of the fresh cell (Fig. S1b) and Li symmetric cell (Fig. S2b) also show comparable features in the charge transfer region, consisting of a single, broad semi-circle. Previous studies have identified Li-ion migration to be the rate determining step in Li metal negative electrodes, while charge transfer and diffusion processes are negligible, suggesting P3 may be closely linked with Li-ion migration [40]. The presence of PSs also influences the Li-ion migration and diffusion characteristics at the anode, indicated by the increase in peak area and time constant of the distribution peaks of a Li||Li cell containing a Li_2S_6 infused electrolyte (Fig. S5). Interestingly, once the Li-S cell begins to discharge, the DRT profile quickly changes; after 2.30 V (Fig. 2b) pseudo peak F3' coalesces with F3 to form a single peak with a significantly reduced overall area. This suggests that an interfacial barrier must be overcome at the Li negative electrode upon cell formation.

The nature of **P4** is more ambiguous than the other peaks, in part due to its appearance as a broad and low magnitude contribution centered between 10^{-3} and 10^{-4} s in the formed cell. In Fig. 1b it has a time constant centered close to 220 μs. No peak appears close to this time constant in the freshly prepared cell (Fig. 2a) or the Li||Li cell (Fig. 3a), where negative electrode contributions are now known to dominate, but small features do appear close to this value in the S||S cell (Fig. 2b 276 μs) and the PS electrolyte C||C cells (Fig. 3c,d) inferring a link to S-based processes and hence the polarisation of the positive electrode.

Peak **P5** lies in the second semicircle of the Nyquist plot of LiS-5 (Fig. 1a) indicating an association with charge transfer reactions [36].

Table 1
Summary of DRT peaks calculated for a Li-S battery at 100% SoC.

DRT Peak	Approximate time constant, τ	Assignment
P1	3 μs	Inter-particle resistance
P2	14.14–28.4 μs	Double-layer relaxation
P3	44.88 μs	Solid-electrolyte interphase
P4	0.3 ms	Positive electrode charge transfer
P5	5 ms	Positive electrode charge transfer
P6	50 ms	Positive electrode charge transfer
P7	0.4 s	Polysulfide diffusion
P8	10 s	Diffusion

In the fresh Li-S cell only a very small feature appears in this region (Fig. 2a), but as the cell is discharged the peak in this zone (F5) becomes significantly more dominant (Fig. 2b–f). The time constant of P5 is 5.51 ms close to the 8.68 ms for F5 (Fig. 2f, 0% SoC) where a maximum R_P is reached and the deposition of insulating Li_2S is complete. This indicates that **P5** is associated with charge transfer at the positive electrode as Li_2S is known to hinder this process. In Fig. 3b, peak S4 occurs at a similar τ value (2.06 ms), but has a very small R_P, which would be expected as carbon and sulfur form intimate composite in this electrode increasing its conductivity.

A characteristic feature of all of the symmetric cells containing PSs (Fig. 3b–d) is a strong feature close to 50 ms. This same feature also appears during the formation of the fresh cell (Fig. 2), but contributions in this region only become significant below 2.13 V where the positive

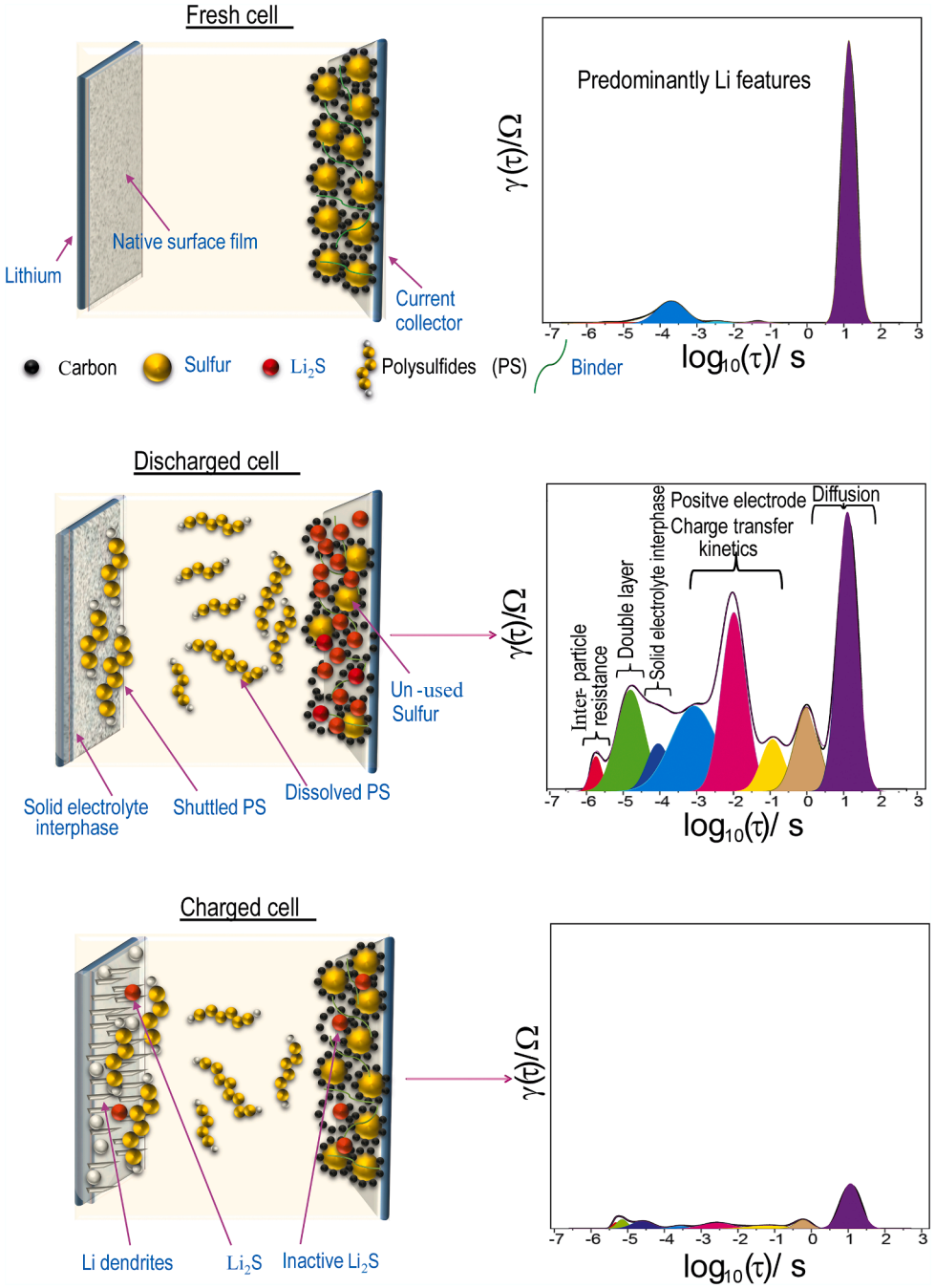

Fig. 4. Schematic representation of the changes in a Li-S cell during charge-discharge and the corresponding evolution of the DRT features (the scale is same in the DRT plots).

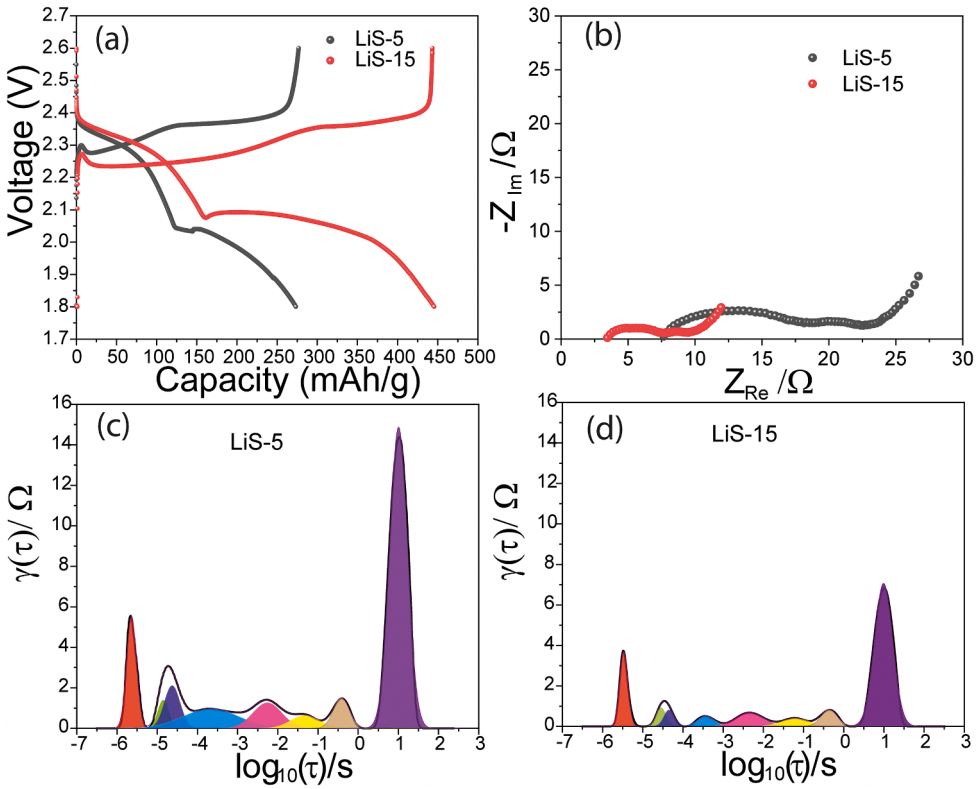

Fig. 5. (a) Charge-discharge curves of LiS-5 and LiS-15 recorded at C/20; (b) Nyquist plots of LiS-5 and LiS-15 measured at 100% SoC; (c) and (d) DRT profiles of the LiS-5 and LiS-15 measured at 100% SoC.

elecyrode and electrolyte are flooded with PSs. Peak **P6** eventually stabilises in this region, which is known to be associated with charge transfer reactions [36], hence this contribution can be linked to the charge transfer of PSs.

It has been noted above that unusually two peaks, **P7** and **P8**, appear in the diffusion region of the DRT profile of a formed cell at 100% SoC (Fig. 1b). In the freshly prepared cell no signature appears in the **P7** region, with a response only appearing at 0.76 s (**F7**), at or below 2.3 V on discharge (Fig. 2b) where PSs are present. A peak appears in this region for the remainder of the discharge (Fig. 2c–f). The DRT of the symmetric C||C paper cells with PS infused electrolytes (Fig. 3d, e) also show a peak at a similar τ (0.46 s for Li_2S_6), suggesting this peak is associated with the diffusion of the PSs in the diffusion layer at the positive electrode [28c]. Interestingly at 2.3 V (Fig. 2b) the diffusion characteristics of the fresh cell are similar to those found in pristine Cu||Li_2S cells (Fig. S3). The Cu||Li_2S cell also shows two peaks, **D1** and **D2**, in the diffusion region at τ values of 1.12 s and 12.23 s, as do the C||C cells with PS infused electrolytes. These observations further support the assertion that **P7** is most likely to be associated with PS diffusion.

In contrast, a very significant peak appears in the area associated with **P8** in the freshly prepared cell, indicating its association with bulk ion-diffusion (Fig. 2a). This is supported by the fact that the polarisation resistance of this ion diffusion peak (at 7.05 s in Fig. 2a) significantly decreases from 162 to 3.70 Ω at 2.3 V, rationalised by the fact that at this potential dissolution of sulfur (sulfur has low ionic conductivity) and formation of PSs causes structural changes in the positive electrode, improving the movement of Li-ions throughout. The diffusion resistance was then observed to increase upon further discharge, after the initial drop, likely due to the deposition of poorly ion-conducting Li_2S (Fig. 2c–f).

DRT profiles calculated upon re-charging the to 100% SoC are shown in Fig. S6. When the cell is brought back to 100% SoC it shows higher polarisation resistances and some shifts in the time constant values. These results indicate that the cell undergoes irreversible changes in the electrode structure and cell properties during both charge-discharge, likely linked to the gradual deposition of Li_2S and PS reduction at the anode.

The assignment of P1–P8 are summarised in Table 1, while the changes in the Li-S cell chemistry as it is discharged from the 100% SoC (fresh cell) to 0% SoC and back again are schematically summarised in Fig. 4.

By understanding these key polarisations, it is possible to dynamically diagnose processes occurring within Li-S cells. The power of this technique is demonstrated below, showing the impact of the electrolyte: sulfur loading on cell performance.

3.2. *DRT analyses of Li-S cells with lean and flooded electrolyte conditions*

To realise the potential of Li-S batteries, their performance must be optimised under lean electrolyte conditions where volumetric and gravimetric energy densities are maximised. Therefore, understanding of the performance-limiting steps in cells with low electrolyte volumes is essential to the commercial progress of Li-S batteries. To this end, *in situ* EIS measurements were performed on cells under lean (LiS-5, 5 $\mu l_{electrolyte}/mg_{sulfur}$) and flooded (LiS-15, 15 $\mu l_{electrolyte}/mg_{sulfur}$) electrolyte conditions and our previous analyses of Li-S DRT profiles were used to understand the performance-limiting electrode reactions. Charge-discharge profiles of the cells measured at C/20 after a formation cycle are shown in Fig. 5a; the cell with lean electrolyte exhibits a capacity of ≈273 mAh g^{-1}, which is only 60% of the capacity obtained with the flooded electrolyte cell (≈445 mAh g^{-1}). A greater capacity is indicative of a higher sulfur utilisation and consistent with an increased volume of electrolyte dissolving more PSs, i.e., forming more catholyte. It should be noted that the commercial sulfur electrodes used here exhibit lower capacities than those reported for lab-made electrodes in

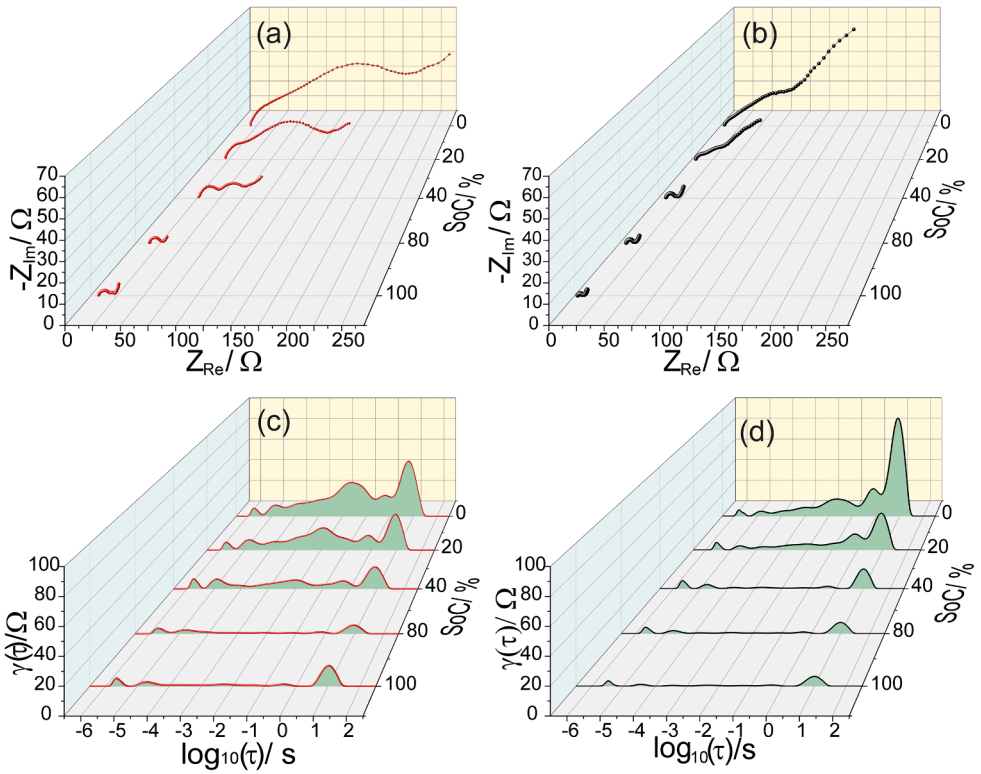

Fig. 6. EIS and DRT analyses at different SoC. (a) and (b) EIS plots of LiS-5 and LiS-15, respectively, recorded at different SoCs; (c) and (d) DRT profiles at different SoC for LiS-5 and LiS-15, respectively.

the literature, however the consistency between electrodes is significantly improved – an essential characteristic for our systematic investigation.

Nyquist plots of the two cells recorded at 100% SoC are presented in Fig. 5b. The LiS-5 cell showed an ESR of 7.67 Ω, roughly double the value of the flooded cell (3.64 Ω). This increased cell conductance is also reflected in the charge-discharge profile of the LiS-15 cell, which shows a higher voltage discharge and lower voltage charge ($E_{cell} = E^{\circ}$-IR, where E° is the standard electrode potential and R is the ESR) [41]. Interestingly, the two systems show significant differences in both their R_{ct} and diffusion profiles, highlighting the impact of the electrolyte content on the charge transfer kinetics; lower R_{ct} values were measured for the LiS-15 cell than the LiS-5. Impedance spectra of both cells yielded two semi-circles: a large semi-circle in the high-frequency region and a small semi-circle in the mid-frequency region, followed by a low-frequency diffusion line. However, these broad generalisations do not allow effects on individual cell process to be evaluated.

The corresponding DRT plots of LiS-5 and LiS-15 are given in Fig. 5c and d, respectively, where the eight local maxima identified as being characteristic of Li-S cells can be observed for each cell. It is important to first note that at 100% SoC (Fig. 5c and d) the features observed here are different from the freshly prepared (pre-formation cycle) cell at 100% SoC (Fig. 2a), indicating that the PSs and Li_2S formed after discharge are not completely converted back to sulfur upon charging.

P1 (inter-particle resistance) at the smallest τ (highest frequency) is significantly larger (higher R_p) for LiS-5 ($R_P = 1.76$ Ω) than LiS-15 ($R_P = 0.926$ Ω). Here it can also be observed that the LiS-15 peak has a slightly greater τ value (3.35 vs 2.28 μs), which can be explained by a higher capacitance caused by the large electrolyte volume, which increases the area of the electrochemical interface ($\tau = RQ^{1/\alpha}$). In fact the R_p for all polarisations in LiS-5 are significantly higher than for LiS-15, indicating all processes in the cell with reduced electrolyte are relatively hindered, and there is also a trend towards slightly higher τ for the LiS-15 peaks also, indicating slow relaxations.

The overall differences noted in the formed 100% SoC cells indicate differences in cell chemistry. Peak P2, identified as the double-layer relaxation at the positive electrode, shows the presence of more PSs at the electrochemical interface in the flooded cell. The PS saturation point of LiS-15 is higher than LiS-5, therefore the PS concentration is higher in LiS-15 and reflected in the peak height and position of P2. P3, which is linked with the polarisation of negative electrode, shows a more resistive SEI may have formed in LiS-5. P4, which highlights the polarisation of sulfur in the positive electrode, suggests faster charge-transfer kinetics in the cell with more electrolyte. The subsequent two peaks (P5 and P6), being indicative of charge-transfer kinetics at the positive electrode, show lower polarisation resistance in LiS-15 than LiS-5 cells, characteristic of faster charge transfer in the cell with more electrolyte. In LiS-15, the positive electrode has more exposed carbon due to the high rate of sulfur dissolution, affording faster electrode kinetics. The same trend can be observed in diffusion resistance region (P7 and P8), with the polarisation resistance (Tables S4 and S5) of the flooded cells being lower than that of the lean electrolyte cell. This trend can be explained by the fact that higher electrolyte volumes enable easier movement of ions to reaction centres, helped by the fact that more sulfur and PSs can dissolve in the LiS-15 cell, resulting in more positive electrode porosity. The increased catholyte concentration in LiS-5 will also result in increased electrolyte viscosity (the effect of dissolved PSs on viscosity is likely more prominent in lean electrolyte conditions), increasing diffusion resistance.

From the above observations, we see that the changes in the cell and electrode properties such as resistance, electrochemical double-layer, charge transfer kinetics, and mass-transfer properties can be straightforwardly analysed by following changes in the position, height and area of the DRT peaks, making it a powerful diagnostic tool for LiS batteries. However, the somewhat uniform changes observed in Fig. 5 cannot be assumed to be universal, as shown by the data in Fig. 2.

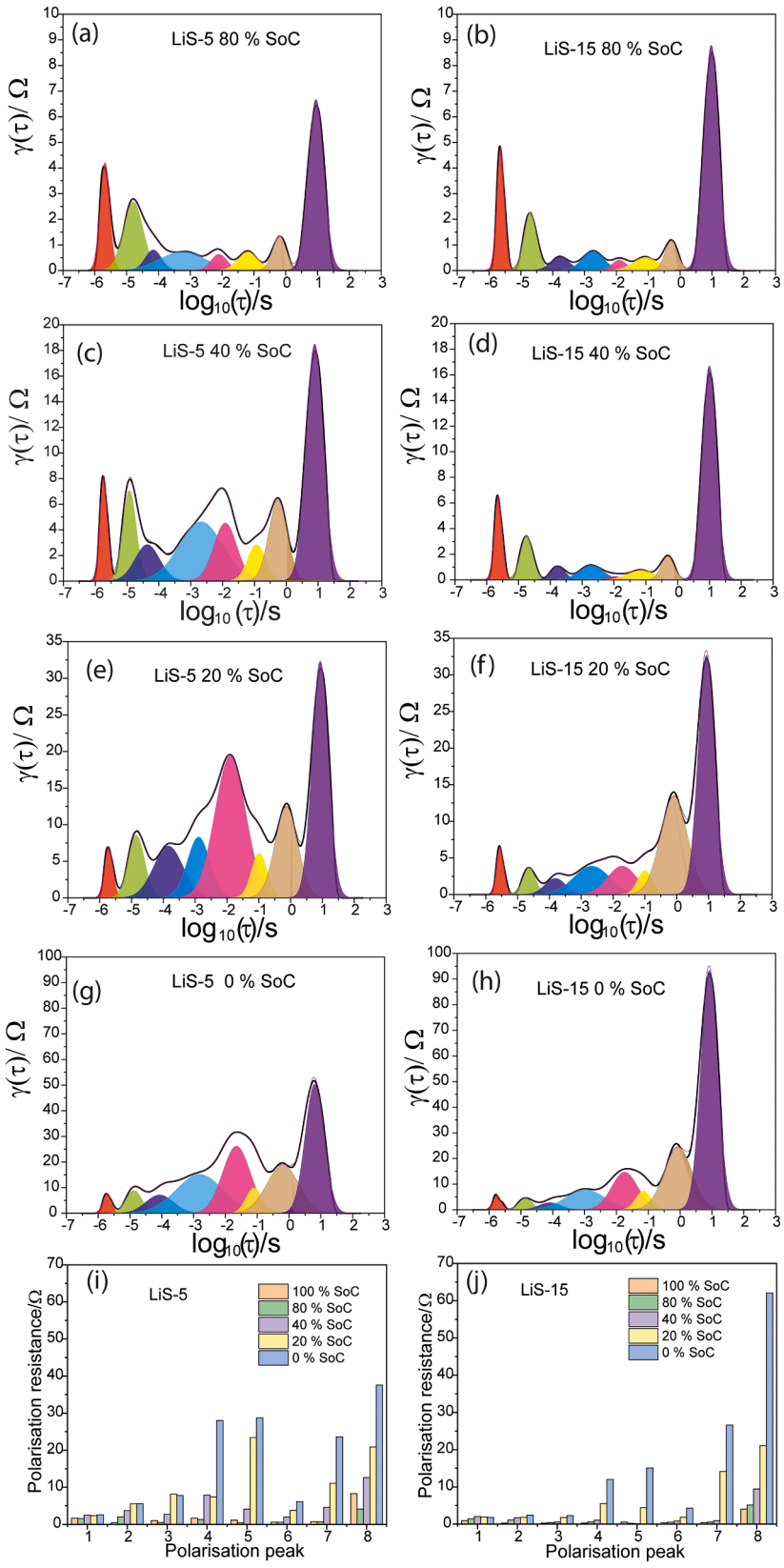

Fig. 7. Comparison of DRT profiles of LiS-5 and LiS-15 at 100, 80, 40, 20, and 0% SoC (a–h) and evolution of R_P of the various electrode processes (P1-8) at different SoCs in LiS-5 and LiS-15 (i, j).

It is well established that Li-S batteries exhibit different electrode reactions at different SoC, hence it was necessary to uncover the impact of electrolyte volume throughout the cell cycle [8]. EIS measurements of LiS-5 (Fig. 6a) and LiS-15 (Fig. 6b) cells, recorded at 100, 80, 40, 20, and 0% SoC after the formation cycle, provide Nyquist plots that show similar features at the same SoC, but with marked differences in their impedance values (See Fig. S7).

The DRT profiles of the EIS measurements at different SoCs for LiS-5 and LiS-15 are shown in Fig. 6c and d, respectively; the R_P values of LiS-5 are higher than the R_P of LiS-15 which correlates well with the EIS measurements. The R_P values show gradual change when the cells are discharged to 80% SoC in LiS-5 and 40% SoC in LiS-15, the respective cells on subsequent discharge show drastic increases in R_P. This suggests that kinetic and mass transfer limitations start to dominate at early stages of discharge under lean electrolyte conditions.

DRT analysis of LiS-5 and LiS-15 at each SoC are shown in Fig. 7a–h. LiS-5 continues the general trend of higher R_P values, showing that lean electrolyte conditions have a substantial effect on the electrode kinetics and mass transfer, but this is not the case for all the polarisations (P1-8) at all SoC (Fig. 7). The different DRT profiles of lean and flooded cells are caused by the varied degree of sulfur and PS solubility, cell conductance and electrochemically inactive solid precipitation. DRT can isolate various electrode polarisations which can be quantitatively measured, thus DRT is better equipped to understand the influence of electrolyte content on the cell behaviour.

At 80% SoC (Fig. 7a and b), an increase in the R_P for LiS-15, and the broadening of the peaks in LiS-5 can be observed, indicating an increase in the polarisation at the electrode surface. The R_P of the ion diffusion (P8) is slightly larger in LiS-15 (5.12 Ω) compared to LiS-5 (4.12 Ω), which can be attributed to the thicker Li_2S layer at the positive electrode (formed during initial charge-discharge); thick Li_2S precipitates have been observed previously in excess electrolyte conditions [12]. At 40% SoC (Fig. 7c and d), when Li_2S_4 to Li_2S_2 conversion is well underway, the peaks characteristic of PS reactions and diffusion exhibit a drastic increase in R_P and are greatly broadened in LiS-5, whereas R_P in the DRT profile of LiS-15 increased only slightly with little broadening, implying that the high electrolyte content can promote faster reaction kinetics. A large volume of electrolyte (LiS-15) can dissolve more polysulfides, which depletes the cathode to a greater extent and exposes more conductive carbon in the process. As the charge transfer reactions are more fissile on the conductive surface, LiS-15 shows a low charge transfer resistance. When cells are discharged to 20% SoC (Fig. 7e and f), the formation of Li_2S from Li_2S_2 is taking place in both the cells; Li_2S is insulating and electrochemically inactive with high ion diffusion resistance. LiS-5 shows very high R_P values (P5 = 23.42 Ω, P6 = 3.7 Ω) for the PS reactions compared to LiS-15 (R_P: P5 = 4.39 Ω, P6 = 1.86 Ω) indicating high polarisation resistance, it appears that the effect of Li_2S_2 deposits is more prominent in the lean electrolyte, which is exacerbated by limited ion diffusion. At this point, the two systems show similar ion diffusion characteristics which indicates electrode kinetics have a more pronounced effect on cell performance than ion diffusion. When the cell is discharged completely to 0% SoC (Fig. 7g and h), the cells show very high R_P values; again the resistance is higher for LiS-5 than LiS-15. However, the R_P of the diffusion resistance (P8) in LiS-15 is almost twice that observed in LiS-5 (62.1 vs 37.5 Ω), which we rationalise by understanding that while discharging, LiS-15 dissolves more PSs, therefore, when the limit of discharge is reached more Li_2S is formed in LiS-15, hence high diffusion resistance. This is evident from the R_P values of P7 (LiS-15 26.5 Ω and LiS-5 23.6 Ω), characteristic of PS diffusion. It can be seen that the diffusion characteristics of a Li-S cell is the complex interplay of the PS concentration in the electrolyte and electrode structure, which is continuously evolving due to PS dissolution and Li_2S_2/Li_2S precipitation as the cell is discharged.

In Fig. 7i–j, the R_P values of polarisations P1-P8 in LiS-5 and LiS-15 are compared. It can be seen that many of the peaks show direct correation with cell SoC. Importantly, it can be observed for both cell compositions several of the peaks (P1-P8) show a direct correlation with cell SoC. This highlights their potential for cell diagnostics. Both P7 and P8 generally have a simple inverse relationship with SoC, with significant and easy to identify changes in $\gamma(\tau)$ and R_p, and are hence excellent candidates for use in battery management systems for Li-S batteries. However, as their origins have now been identified, the unique 'fingerprint' of P1-P8 means that their use in the detection of specific modes of cell change, evolution and degradation also offers great potential for on-board battery metrology.

4. Conclusion

This work has deconvoluted the EIS spectrum of Li-S batteries using DRT analysis, identifying eight characteristic local maxima associated with inter-particle resistance, double layer relaxations, negative electrode polarisations, positive electrode polarisations, and ion diffusion resistances. These features represent a 'fingerprint' for the Li-S cell. Importantly, through DRT analysis of pristine cells and those at different SoC, we found that the impedance response of a Li-S battery is dominated by the positive electrode after the initial charge-discharge, whereas the impedance features of a pristine cell are dominated by the Li metal negative electrode. During the cell formation cycles the position, magnitude and number of peaks are somewhat in flux and importantly the cell does not recover its original cell configuration when charged after first discharge, which was reflected in the DRT analysis. However, a consistent DRT profile emerged post-formation, enabling the use of this technique for reliable diagnosis of cell change; DRT profiles of Li-S batteries showed a strong, systematic dependences on the SoC and several other battery parameters.

Investigations of lean and flooded electrolyte cells showed that high electrolyte content improves electrode kinetics and ion diffusion, affording them high capacity, whereas in lean electrolyte conditions high polarisation resistance throughout discharge was observed. To enable lean electrolytes in practical cells, dead volume in the positive electrode should be minimised along with enhancement in electrolyte wettability, and electrolyte formulations should be designed to maximize the utilisation of sulfur. These valuable findings can guide the development of durable and efficient Li-S batteries [42].

More widely, the results presented here demonstrate the power of the DRT method to analyse complex electrochemical systems, and should aid in the study of other emerging energy storage chemistries including Na-S batteries, Zn ion batteries, metal-air batteries and more.

Author contributions

Roby Soni conceived the idea along with Thomas Miller and Alexander Rettie. Roby Soni performed experiments. James Robinson, Dan Brett and Paul Shearing participated in technical discussions. Data analysis was performed by Roby Soni, Alexander Rettie and Thomas Miller, who also drafted and edited the manuscript. This project was supervised by Thomas Miller and Alexander Rettie.

Declaration of Competing Interest

The authors declare no conflicting interests.

Acknowledgments

This work was supported by the Faraday Institution (www.faraday.ac.uk; EP/S003053/1) through the Lithium Sulfur Technology Accelerator (LiSTAR) programme (FIRG014). P.R.S. acknowledges The Royal Academy of Engineering (CiET1718/59).

Supplementary materials

Supplementary material associated with this article can be found, in

the online version, at doi:10.1016/j.ensm.2022.06.016.

References

[1] A. Manthiram, Y. Fu, S.H. Chung, C. Zu, Y.S. Su, Rechargeable lithium–sulfur batteries, Chem. Rev. 114 (2014) 11751–11787.

[2] J. Park, B.C. Yu, J.S. Park, J.W. Choi, C. Kim, Y.E. Sung, J.B. Goodenough, Tungsten disulfide catalysts supported on a carbon cloth interlayer for high performance Li–S battery, Adv. Energy Mater. 7 (2017), 1602567.

[3] H. Lin, S. Zhang, T. Zhang, S. Cao, H. Ye, Q. Yao, G.W. Zheng, J.Y. Lee, A cathode-integrated sulfur-deficient Co9S8 catalytic interlayer for the reutilization of "lost" polysulfides in lithium–sulfur batteries, ACS Nano 13 (2019) 7073–7082.

[4] X. Ji, K.T. Lee, L.F. Nazar, A highly ordered nanostructured carbon–sulphur cathode for lithium–sulphur batteries, Nat. Mater. 8 (6) (2009) 500–506.

[5] L. Suo, Y.S. Hu, H. Li, M. Armand, L. Chen, A new class of solvent-in-salt electrolyte for high-energy rechargeable metallic lithium batteries, Nat. Commun. 4 (1) (2013) 1481.

[6] S. Evers, L.F. Nazar, Graphene-enveloped sulfur in a one pot reaction: a cathode with good coulombic efficiency and high practical sulfur content, Chem. Commun. 48 (9) (2012) 1233–1235.

[7] G. Zheng, Y. Yang, J.J. Cha, S.S. Hong, Y. Cui, Hollow carbon nanofiber-encapsulated sulfur cathodes for high specific capacity rechargeable lithium batteries, Nano Lett. 11 (10) (2011) 4462–4467.

[8] M. Wild, L. O'Neill, T. Zhang, R. Purkayastha, G. Minton, M. Marinescu, G.J. Offer, Lithium sulfur batteries, a mechanistic review, Energy Environ. Sci. 8 (2015) 3477–3494.

[9] (a) S. Wang, J. Zhang, O. Gharbi, V. Vivier, M. Gao, M.E. Orazem, Electrochemical impedance spectroscopy, Nat. Rev. Methods Prim. 1 (2021) 1–21;
(b) P. Vadhva, J. Hu, M.J. Johnson, R. Stocker, M. Braglia, D.J.L. Brett, A.J. E. Rettie, Electrochemical impedance spectroscopy for all-solid-state batteries: theory, methods and future outlook, ChemElectroChem 8 (2021) 1930–1947.

[10] N.A. Cañas, K. Hirose, B. Pascucci, N. Wagner, K.A. Friedrich, R. Hiesgen, Investigations of lithium–sulfur batteries using electrochemical impedance spectroscopy, Electrochim. Acta 97 (2013) 42–51.

[11] Z. Deng, Z. Zhang, Y. Lai, J. Liu, J. Li, Y. Liu, Electrochemical impedance spectroscopy study of a lithium/sulfur battery: modeling and analysis of capacity fading, J. Electrochem. Soc. 160 (2013) A553–A558.

[12] Z. Guo, H. Nie, Z. Yang, W. Hua, C. Ruan, D. Chan, M. Ge, X. Chen, S. Huang, 3D CNTs/graphene-S-Al_3Ni_2 cathodes of high-sulfur-loading and long-life lithium-sulfur batteries, Adv. Sci. 5 (2018), 1800026.

[13] J. Yan, X. Liu, B. Li, Capacity fade analysis of sulfur cathodes in lithium–sulfur batteries, Adv. Sci. 3 (2016), 1600101.

[14] A. Kilic, D. Eroglu, Characterization of the effect of cell design on Li−S battery resistance using electrochemical impedance spectroscopy, ChemElectroChem 8 (2021) 963–971.

[15] B.A. Boukamp, Distribution (function) of relaxation times, successor to complex nonlinear least squares analysis of electrochemical impedance spectroscopy? J. Phys. Energy 2 (2020), 042001.

[16] C. Montella, Voigt circuit representation model for electrochemical impedances under finite-length diffusion conditions, J. Electroanal. Chem. 879 (2020), 114785.

[17] Y. Zhang, Y. Chen, M. Yan, F. Chen, Reconstruction of relaxation time distribution from linear electrochemical impedance spectroscopy, J. Power Sources 283 (2015) 464–477.

[18] J. Schneider, T. Tichter, P. Khadke, R. Zeis, C. Roth, Deconvolution of electrochemical impedance data for the monitoring of electrode degradation in VRFB, Electrochim. Acta 336 (2020), 135510.

[19] A.D. Franklin, H.J. De Bruin, The fourier analysis of impedance spectra for electroded solid electrolytes, phys. Status Solidi A 75 (1983) 647–656.

[20] H. Qi, T. Yang, W. Li, L. Ma, S. Hu, W. Shi, E.M. Sabolsky, J.W. Zondlo, R. Hart, G. A. Hackett, X. Liu, Reversible *in-situ* exsolution of Fe catalyst in $La_{0.5}Sr_{1.5}Fe_{1.5}Mo_{0.5}O_{6-\delta}$ anode for SOFCs, ECS Trans. 91 (2019) 1701–1710.

[21] Y. Zhang, Y. Chen, F. Chen, *In-situ* quantification of solid oxide fuel cell electrode microstructure by electrochemical impedance spectroscopy, J. Power Sources 277 (2015) 277–285.

[22] J. Hong, A. Bhardwaj, H. Bae, I.H. Kim, S.J. Song, Electrochemical impedance analysis of SOFC with transmission line model using distribution of relaxation times (DRT), J. Electrochem. Soc. 167 (2020), 114504.

[23] A. Kulikovsky, PEM fuel cell distribution of relaxation times: a method for the calculation and behavior of an oxygen transport peak, Phys. Chem. Chem. Phys. 22 (2020) 19131–19138.

[24] M. Heinzmann, A. Weber, E. Ivers-Tiffée, Advanced impedance study of polymer electrolyte membrane single cells by means of distribution of relaxation times, J. Power Sources 402 (2018) 24–33.

[25] J.G. Lyagaeva, G.K. Vdovin, D.A. Medvedev, Distinguishing bulk and grain boundary transport of a proton-conducting electrolyte by combining equivalent circuit scheme and distribution of relaxation times analyses, J. Phys. Chem. C 123 (2019) 21993–21997.

[26] M. Hahn, D. Rosenbach, A. Krimalowski, T. Nazarenus, R. Moos, M. Thelakkat, M. A. Danzer, Investigating solid polymer and ceramic electrolytes for lithium-ion batteries by means of an extended distribution of relaxation times analysis, Electrochim. Acta 344 (2020), 136060.

[27] J.P. Schmidt, P. Berg, M. Schönleber, A. Weber, E. Ivers-Tiffée, The distribution of relaxation times as basis for generalized time-domain models for Li-ion batteries, J. Power Sources 221 (2013) 70–77.

[28] (a) S. Risse, N.A. Cañas, N. Wagner, E. Härk, M. Ballauff, K.A. Friedrich, Correlation of capacity fading processes and electrochemicalimpedance spectra in lithium/sulfur cells, J. Power Sources 323 (2016) 107–114;
(b) M. Gerle, N. Wagner, J. Hacker, M. Nojabaee, K.A. Friedrich, Identification of the underlying processes in impedance response of sulfur/carbon composite cathodes at different SOC, J. Electrochem. Soc. 169 (2022) 30505;
(c) Y.N. Song, Y.Q. Peng, M. Zhao, Y. Lu, J.N. Liu, B.Q. Li, Q. Zhang, Understanding the impedance response of lithium polysulfide symmetric cells, Small Sci. 1 (2021), 210042.

[29] S. Risse, E. Hark, B. Kent, M. Ballauff, Operando analysis of a lithium/sulfur battery by small-angle neutron scattering, ACS Nano 13 (2019) 10233–10241.

[30] M. Hahn, S. Schindler, L.C. Triebs, M.A. Danzer, Optimized process parameters for a reproducible distribution of relaxation times analysis of electrochemical systems, Batteries 5 (2019) 43–64.

[31] T.H. Wan, M. Saccoccio, C. Chen, F. Ciucci, Influence of the discretization methods on the distribution of relaxation times deconvolution: implementing radial basis functions with DRTtools, Electrochim. Acta 184 (2015) 483–499.

[32] S. Waluś, C. Barchasz, R. Bouchet, F. Alloin, Electrochemical impedance spectroscopy study of lithium–sulfur batteries: useful technique to reveal the Li/S electrochemical mechanism, Electrochim. Acta 359 (2020), 136944.

[33] S. Gadoue, K. Chen, P. Mitcheson, V. Yufit, N. Brandon, Electrochemical impedance spectroscopy state of charge measurement for batteries using power converter modulation, in: Proceedings of the 9th International Renewable Energy Congress (IREC), 2018, pp. 1–5, 20-22 March.

[34] X. Qiu, Q. Hua, L. Zheng, Z. Dai, Study of the discharge/charge process of lithium–sulfur batteries by electrochemical impedance spectroscopy, RSC Adv. 10 (2020) 5283–5293.

[35] J.R. Macdonald, W.B. Johnson, Fundamentals of impedance spectroscopy. Impedance Spectroscopy, John Wiley & Sons, Inc., 2018, pp. 1–20.

[36] M.A. Danzer, Generalized distribution of relaxation times analysis for the characterization of impedance spectra, Batteries 5 (2019) 53–68.

[37] J. Conder, C. Villevieille, S. Trabesinger, P. Novák, L. Gubler, R. Bouchet, Electrochemical impedance spectroscopy of a Li–S battery: part 1. Influence of the electrode and electrolyte compositions on the impedance of symmetric cells, Electrochim. Acta 244 (2017) 61–68.

[38] S. Choi, I. Yoon, W.T. Nichols, D. Shin, Carbon-coated Li_2S cathode for improving the electrochemical properties of an all-solid-state lithium-sulfur battery using Li_2S-P_2S_5 solid electrolyte, Ceram. Int. 44 (7) (2018) 7450–7453.

[39] H. Ye, M. Li, T. Liu, Y. Li, J. Lu, Activating Li_2S as the lithium-containing cathode in lithium–sulfur batteries, ACS Energy Lett. 5 (7) (2020) 2234–2245.

[40] D. Aurbach, Review of selected electrode-solution interaction which determine the performance of Li and Li ion batteries, J. Power Sources 89 (2) (2000) 206–218.

[41] M. Park, X. Zhang, M. Chung, G.B. Less, A.M. Sastry, A review of conduction phenomena in Li-ion batteries, J. Power Sources 195 (2010) 7904–7929.

[42] James Robinson B., et al., 2021 roadmap on lithium sulfur batteries, J. Phys.: Energy 3 (3) (2021), 031501, https://doi.org/10.1088/2515-7655/abdb9a.